DOI: 10.1002/chem.200801131

Electronic Structure, Chemical Bonding, and Solid-State NMR Spectroscopy of the Digallides of Ca, Sr, and Ba

Frank Haarmann,* Katrin Koch, Daniel Grüner, Walter Schnelle, Oliver Pecher, Raul Cardoso-Gil, Horst Borrmann, Helge Rosner, and Yuri Grin[a]

Abstract: Combined application of ^{69,71}Ga NMR spectroscopy and quantum mechanical calculations reveals the chemical bonding in the digallides of Ca, Sr, and Ba. An analysis of the electron localization function (ELF) shows honeycomb-like 6^3 nets of the Ga atoms as the most prominent structural features in $SrGa_2$ and $BaGa_2$. For $CaGa_2$ a description of a 3+1-coordinated Ga atom is revealed by the ELF and by an analysis of interatomic distances. The NMR spectroscopic signal shift is mainly due to the Knight shift and is almost equal for the investigated digallides, whereas the anisotropy of the signal shift decreases with the radius of the alkaline-earth metals. Calculated and observed values of the electric field gradient (EFG) are in good agreement for $CaGa_2$ and $BaGa_2$ but differ by about 21% for $SrGa_2$ indicating structural instability. Better agreement is achieved by considering a puckering of the Ga layers. For $BaGa_2$ an instability of the structure is indicated by a peak in the density of states at the Fermi level, which is shifted to lower energies when taking puckering of the Ga layers into account. Both structural modifications are confirmed by crystallographic information. The Fermi velocity of the electrons is strongly anisotropic and is largest in the (001) plane of the crystal structure. This results in an alignment of the crystallites with the [001] axis perpendicular to the magnetic field as observed in ^{69,71}Ga NMR spectroscopy and magnetic susceptibility experiments. The electron transport is predominantly mediated by the Ga–Ga p_x- and p_y-like electrons in the (001) plane. The specific heat capacity of $BaGa_2$ was determined and indicated the absence of phase transitions between 1.8 and 320 K.

Keywords: ab initio calculations · electronic structure · intermetallic compounds · NMR spectroscopy · X-ray diffraction

Introduction

Although the chemical bonding of ionic and covalently bonded materials is relatively well understood, this is not the case for intermetallic compounds. To improve these technologically relevant materials systematically a fundamental knowledge of their atomic interactions is desirable, which can only be achieved through the combined application of experimental and theoretical methods. For the sake of clarity we focus in this first study on simple binary compounds as model systems.

The gallides of the alkaline-earth metals show structural features similar to that of Zintl phases, for example, polyanionic components formed by the gallium atoms and isolated cations. Although the digallides of the alkaline-earth metals in first approximation obey simple counting rules, for example, the "8–*N* rule", this is not the case for the other gallides of the alkaline-earth metals, which are the focus of our interest.

Gallium is located in group 13 of the periodic system at the Zintl border.[1] Focusing on the alkaline-earth metals Ca, Sr, and Ba, a high flexibility of gallium with respect to chemical bonding is observed. For example, isolated Ga atoms are found in the crystal structures of $Ca_{28}Ga_{11}$ and $Ba_{10}Ga$.[2,3] Two- and three-bonded Ga atoms forming molecular units are observed in Sr_8Ga_7 and Ba_8Ga_7.[4] Three-dimensional (3D) frameworks are formed by four- and five-bonded Ga atoms in MGa_4 with M = Ca, Sr, or Ba.[5] The transition from 3D frameworks to planar 2D nets of Ga atoms is realized in the homogeneity range of $Sr_{1-x}Ga_{2+3x}$.[6] Triangular Ga_3 units substitute the cations and connect the

[a] Dr. F. Haarmann, Dipl.-Phys. K. Koch, Dr. D. Grüner, Dr. W. Schnelle, Dipl.-Chem. O. Pecher, Dr. R. Cardoso-Gil, Dr. H. Borrmann, Dr. H. Rosner, Prof. Dr. Yu. Grin
Max-Planck-Institut für Chemische Physik fester Stoffe
Nöthnitzer Straße 40, 01187 Dresden (Germany)
Fax: (+49) 351-4646-4002
E-mail: haarmann@cpfs.mpg.de

 © 2009 Wiley-VCH Verlag GmbH & Co. KGaA, Weinheim WILEY InterScience DISCOVER SOMETHING GREAT

layers by forming four-bonded Ga atoms initially found in $YbGa_{2.63}$,[7] $Eu_{1-x}Ga_{2+3x}$,[8] and $Eu_{3-x}Ga_{8+3x}$.[9] A similar substitution of the Sr atoms is realized in $Sr_{3-x}Ga_{8+3x}$ with $x = 0.15$, in which a 3D framework is built by three-, four-, and five-bonded Ga atoms.[10] The change of the coordination number of the Ga atoms from three to four in $M_{1-x}Ga_{2+3x}$ with M = Sr, Yb, and Eu was concluded from the interpretation of the electron density obtained from X-ray diffraction data. However, this data requires verification by independent experiments, thus NMR spectroscopy was chosen for this task.

The gallides of Ca, Sr, and Ba with composition 1:2 have similar crystal structures.[11] $SrGa_2$ and $BaGa_2$ crystallize in a AlB_2-type structure[12] and $CaGa_2$ in a $CaIn_2$-type structure[13] (Figure 1). Three Ga–Ga contacts of 2.51 and 2.56 Å

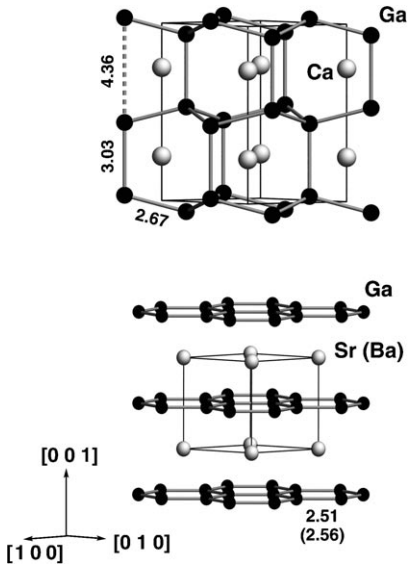

Figure 1. Crystal structures of $CaGa_2$ (top) and $SrGa_2$ and $BaGa_2$ (both bottom). The unit cells are highlighted in black and the Ga–Ga contacts are in gray.

within the 2D Ga layers of the AlB_2-type structure are observed in the digallides of Sr and Ba, respectively. These distances are shorter than the average distance of 2.70 Å in α-Ga.[14] The next-neighbor distances of the Ga atoms in $CaGa_2$ are increased to d(Ga–Ga) = 2.67 Å within the puckered layers. Between the puckered layers the distances are 3.03 and 4.36 Å, which is long compared with the average distance in α-Ga. From the interatomic distances the digallide of calcium can be understood to be an intermediate in the transition from 2D nets towards 3D frameworks by formation of a 3+1 coordination for the Ga atoms.

NMR of nuclei with $I > 1/2$ is sensitive to chemical bonding through the interaction of the nuclear quadrupole moment and the electric-field gradient (EFG) at the nucleus. A deviation of the charge distribution from cubic symmetry in the vicinity of the observed nuclei results in a characteristic change of the line shape of the NMR spectroscopy signals.[15] The quadrupole coupling parameter can be determined by line-shape analysis of the NMR spectroscopy signals and independently obtained from quantum mechanical calculations.[16,17] This combination of experiment and theory can be used to study and understand details of the crystal structure and the chemical bonding. In particular, a combination of NMR spectroscopy and quantum mechanical calculations of the EFG can be used to study local ordering of the atoms, as frequently observed in intermetallic compounds. In this case NMR spectroscopy as a local method provides experimental information about local arrangements of the atoms hardly accessible by other methods. These can be combined with EFG calculations that apply models of local ordering, which are based on the results of accurate X-ray diffraction experiments. In any case, the material used in these studies has to be well characterized to avoid ambiguity. Thus, as a first approach to this strategy ^{69,71}Ga NMR spectroscopy and quantum mechanical calculations were applied to study the peculiarities of the atomic interactions in well-characterized samples of MGa_2 with M = Ca, Sr, and Ba.

Experimental Section

Sample preparation: The samples were prepared by melting appropriate mixtures of the elements in a high-frequency furnace using sealed Ta ampoules to avoid evaporation of the elements (Ca 99.987%, Sr 99.95%, and Ba 99.9% from Alfa Aesar; and Ga 99.999% from ChemPur). Subsequent thermal annealing was carried out on samples in evacuated quartz glass ampoules. The Sr and Ba compounds were treated for 7 d at 900 °C. The samples of composition 1:2 were cooled over 24 h to ambient temperature to ensure local ordering of the atoms. Samples of composition $MGa_{2\pm x}$ with M = Ca, Sr, and Ba were quenched in ice water to obtain information about the phases at the annealing temperature. The Ca compounds were annealed for 5 d at 750 °C, cooled over 10 h to 550 °C, held for 5 d at this temperature, and cooled over 48 h to ambient temperature.

Sample characterization: To ensure single-phase materials for the NMR spectroscopy analyses and measurements of the magnetic susceptibility, the samples were characterized by means of various techniques.

X-ray diffraction was performed on powder samples using a Huber Guinier G670 diffractometer with $Cu_{K\alpha 1}$ radiation ($\lambda = 1.540598$ Å, internal standard LaB_6, $a = 4.15692$ Å). The lattice parameters were determined by using the same set of reflections for a whole series of samples. Single-crystal X-ray diffraction analyses were carried out on $Sr_{1-x}Ga_{2+3x}$ with $x = 0$ and on $BaGa_2$ by using a Rigaku R-Axis Spider diffractometer with rotating anode source ($Ag_{K\alpha}$ radiation) monochromatized and focused by an OSMIC VariMax MR optic. High-temperature powder X-ray diffraction was carried out on $CaGa_2$. A STOE STAPI MP setup with a high-temperature attachment was used in Debye–Scherrer geometry with $Cu_{K\alpha 1}$ radiation ($\lambda = 1.540598$ Å, Ge monochromator). The sample was sealed in a quartz glass capillary.

All samples of composition 1:2 were investigated by means of differential scanning calorimetry (DSC) using a Netzsch DSC 404 C Pegasus with DSC sample holder. The measurements were performed in sealed Nb ampoules to avoid evaporation of the compounds at elevated temperatures.

Metallographic analysis was performed by using optical microscopy. The compositions of the phases were investigated by using energy-dispersive X-ray spectroscopy (EDXS; scanning electron microscope Philips SX 30) and wavelength-dispersive X-ray spectroscopy (WDXS; EPMA CAMECA SX 100; MGa_4 with M = Ca, Sr, and Ba as standards).

 © 2009 Wiley-VCH Verlag GmbH & Co. KGaA, Weinheim

NMR spectroscopy

Data analysis: The line shape of a NMR spectroscopy signal was determined by the chemical shift, Knight shift, core polarization, quadrupole coupling, and/or dipolar couplings.[15] The chemical shift, Knight shift, and core polarization are designated as "shift interactions" in the following.

In the case of large quadrupole coupling the line shape is often dominated by quadrupole coupling only. Nevertheless, in a large magnetic field shift interactions also have to be considered. Compared with the other couplings the dipolar coupling is of minor importance.

Each of the couplings is described by a tensor of second rank in its separate interaction frame, the so-called principal axis system (PAS). The orientation of the various PASs with respect to the crystal axis system (CAS) can be fixed by the site symmetry of the atoms. Their orientations are equal for the Ga positions in $CaGa_2$ ($3m$) and MGa_2 with M = Sr and Ba ($\bar{6}m2$).

The interaction of the nuclear quadrupole moment (Q) with the electric-field gradient (EFG) in a noncubic environment is described by the quadrupole coupling constant (C_Q) defined as $C_Q=(e^2qQ)/h$, in which $eq=V_{ZZ}$ and h = Planck's constant, and by the asymmetry parameter $\eta_Q=(V_{YY}-V_{XX})/V_{ZZ}$ using $|V_{ZZ}|\geqq|V_{XX}|\geqq|V_{YY}|$.[18] V_{XX}, V_{YY}, and V_{ZZ} are the eigenvalues of the traceless quadrupole coupling tensor. To avoid confusion we emphasize that the definition of the asymmetry parameter applied in the SIMPSON program used for least-squares fitting and simulation of the NMR spectroscopy signals differs from that introduced by Abragam: $\eta_Q=(V_{XX}-V_{YY})/V_{ZZ}$ using $|V_{ZZ}|\geqq|V_{YY}|\geqq|V_{XX}|$.[19] The nuclear quadrupole moments of both Ga isotopes used for evaluation of the data are $Q(^{69}\mathrm{Ga})=17.1$ fm^2 and $Q(^{71}\mathrm{Ga})=10.7$ fm^2 (ref. [20]).

The shift interactions can be due to orbital motion of the electrons (chemical shielding, δ), coupling of nuclear and electron spins, and/or polarization of the core electrons. The latter two are known as Knight shift (K) and their origin cannot be resolved by means of analysis of the line shape. The shift interactions will be described by three quantities: isotropic shift (Δ_{iso}), anisotropy (Δ_{aniso}), and asymmetry parameter (η_Δ). Because of the site symmetry of the Ga positions in the digallides of Ca, Sr, and Ba the equation $\eta_Q=\eta_\Delta=0$ results.

The orientation dependence of the various interactions produces a characteristic frequency distribution for the NMR spectroscopy signal of a powder composed of randomly oriented crystallites (regular powder) as well as for a powder of crystallites with preferred orientation (oriented powder). The NMR spectroscopy signal of a nucleus with nuclear spin $I=3/2$ is composed of the main and two satellite transitions. The main transition shows a characteristic orientation dependence only in the case of large quadrupole coupling, which is described by second-order perturbation theory. The satellite transitions cover a broad frequency range whereas the main transition remains almost in the center. All transitions are influenced by the shift interactions as well. However, the quadrupole coupling constant can be unambiguously determined in the present case for $\eta_Q=0$ by certain frequencies—the so-called singularities—of the satellite transitions, as can be shown by simulations of the signals. The frequency difference of the singularities remains constant independent of the shift interactions. For large quadrupole coupling, as presented here, it is often only possible to measure the frequency of these characteristic features that have the largest intensity.

Measurement techniques: The NMR spectroscopy investigations were performed at ambient temperature by using a Bruker AVANCE spectrometer with magnetic field of $\mu_0H=11.74$ T. The corresponding frequencies of the ^{69}Ga and the ^{71}Ga isotopes are 120.099 and 152.526 MHz, respectively. The Ga signals are referenced to a solution of $Ga(NO_3)_3$ in D_2O.

The compounds were embedded in two-component glue (UHU endfest 300) and filled in quartz glass tubes of 5 mm diameter for experiments on regular powder and oriented powder of MGa_2 with M = Ca, Sr, and Ba. Alignment of the crystallites was achieved by exposing the samples to a magnetic field of $\mu_0H=11.74$ T during the hardening process of the glue. The samples were mounted on a low-Q wide-line probe equipped with a one-cycle goniometer of angular precision $\pm2°$ built by NMR-Service (Erfurt, Germany).

Due to the large total width of the signals the characteristic frequency ranges of spectra were separately measured in three experiments using different carrier frequencies. These frequency ranges contain the representative features of largest intensity of the satellite transitions and the whole main transition.

An echo sequence with pulses of equal duration was applied in all experiments for the detection of the signals. The interpulse distance was optimized to avoid distortions of the line shape for the main transition to 60 μs and for the satellite transitions to 30 μs.

For wide-line measurements of oriented and nonoriented samples high-intensity pulses of a duration of 1.5 μs were employed. To avoid serious line-shape distortions of the broad ^{69}Ga main transition in $SrGa_2$, a series of selective excitation experiments was applied by using low-power pulses with a duration of $\tau(\pi/2)=50$ μs. All experiments were performed by using eight-fold cycles of the pulse sequences.

Magnetic susceptibility: Magnetization was measured in a SQUID magnetometer (MPMS XL-7, Quantum Design) in various high magnetic fields up to $\mu_0H=7$ T. The magnetic susceptibility $\chi=M/H$ (M = magnetization, H = magnetic field strength) was determined for powder samples enclosed in quartz glass tubes. The samples were either filled loosely into the tubes or suspended in liquid paraffin. The tubes with and without paraffin were calibrated prior to filling by using the automatic background-subtraction feature of the magnetometer software. After mixing the sample with the liquid paraffin the crystallites are assumed to be randomly oriented. After the first set of magnetization measurements the sample temperature was raised well above the melting point of the paraffin while shaking the sample with the RSO drive of the magnetometer in the maximum field ($\mu_0H=7$ T). These samples were assumed to have oriented crystallites. All manipulations were performed under an inert atmosphere.

Heat capacity: The heat capacity (C_p) of a piece of $BaGa_2$ ($m=14.51$ mg) was determined by using a relaxation method (PPMS, Quantum Design) between 1.8 and 320 K. The sample was attached with a minute amount of Apiezon N grease to the sapphire sample holder of the option puck of the instrument. Exposure to air could be minimized to the few seconds that were necessary for lowering the puck into the cryostat.

Calculation procedures: The electronic-structure calculations were performed with two different codes. The optimization of the structural parameters was done with the full-potential local-orbital minimum basis code (FPLO) (version 5.00–19)[21] within the local density approximation (LDA). In the scalar relativistic calculations the exchange and correlation potential of Perdew and Wang[22] was employed. The basis sets Ga(3s3p/4s4p3d), Ba(4s4p4d5s5p/6s6p5d), Sr(3s3p3d4s4p/5s5p4d), and Ca(3s3p/4s4p3d) were chosen for semicore/valence states. The lower-lying states were treated fully relativistically as core states. In the irreducible part of the Brillouin zone 455 k points for $CaGa_2$, 432 k points for $SrGa_2$, and 504 k points for $BaGa_2$ were used.

The electric-field gradient and density of states (DOS) were calculated with the full-potential linearized augmented plane wave plus local orbitals (LAPW+lo) code WIEN2k[23] using the optimized structural parameters. To be consistent, the exchange and correlation potential of Perdew and Wang and the same number of irreducible k points as for the optimization of the lattice parameters were used.

The chosen atomic sphere radii (R_{MT}) were 2.5 a.u. for M; and $R_{MT}=2.46$ a.u. in $CaGa_2$, $R_{MT}=2.33$ a.u. in $SrGa_2$, and $R_{MT}=2.38$ a.u. in $BaGa_2$ for Ga. The number of basis functions was determined by a value of $R_{MT}K_{max}$ of 8.5 in all compounds (K_{max} = magnitude of the largest K vector). The separation energy was set to −6.0 Ry by treating Ga(3d4s4p), Ba(5s5p6s), Sr(4s4p5s), and Ca(3s3p4s) as semicore and valence states. The maximum l value for partial waves inside the atomic spheres was set to 10.

Additional calculations of the electric-field gradients were done using FPLO (version 5.00–19)[21] for super structure models of the AlB_2-type structure with an experimental and optimized lattice parameter. Furthermore, a comparison within the generalized gradient approximation (GGA) was done in the same way. A calculation of the Fermi surfaces was done with FPLO by applying the optimized lattice parameter.

 © 2009 Wiley-VCH Verlag GmbH & Co. KGaA, Weinheim

The electron localization function (ELF) was evaluated according to ref. [24] within the FPLO program package with an ELF module,[25] and was analyzed with the program Basin.[26] For the ELF calculations, the optimized unit-cell parameters were used. No significant differences were observed by comparing the ELF of optimized and nonoptimized unit-cell parameters for $SrGa_2$.

Results and Discussion

Crystal chemistry of the digallides of Ca, Sr, and Ba: Samples of stoichiometric composition 1:2 are single-phase materials, whereas those of nominal compositions $Ca_{1.05}Ga_2$, $Ca_{0.98}Ga_2$, $Ba_{1.1}Ga_2$, and $Ba_{0.9}Ga_2$ are two-phase materials. Within the experimental error the lattice parameters of the two- and single-phase samples of MGa_2 with M = Ca and Ba are equal, which indicates the absence of a significant homogeneity range (Table 1). The Sr compound differs by possessing a homogeneity range $Sr_{1-x}Ga_{2+3x}$ with $0 \le x \le 0.076$ at 950 °C.[6] Metallographic observations agree well with these results. For the remaining part of the manuscript we will focus on the compounds with stoichiometric composition 1:2 and denote the sample $Sr_{1-x}Ga_{2+3x}$ with $x = 0$ as $SrGa_2$.

Table 1. Observed (obsd) and optimized (calcd) lattice parameters, and relative deviation (dev) for the alkaline-earth metal digallides of Ca, Sr, and Ba.

	a(obsd) [Å]	*a*(calcd) [Å]	dev [%]	*c*(obsd) [Å]	*c*(calcd) [Å]	dev [%]
$Ca_{1.05}Ga_2$	4.4726(2)	–	–	7.3868(4)	–	–
$Ca_{1.00}Ga_2$	4.4714(1)	4.3982	−1.7	7.3920(7)	7.1206	−3.6
$Ca_{0.98}Ga_2$	4.4716(3)	–	–	7.3874(7)	–	–
$Sr_{1.00}Ga_2$	4.3484(2)	4.2911	−1.3	4.7360(5)	4.5470	−4.0
$Ba_{1.10}Ga_2$	4.4328(6)	–	–	5.0809(8)	–	–
$Ba_{1.00}Ga_2$	4.4322(1)	4.3933	−0.9	5.0824(6)	4.8970	−3.6
$Ba_{0.90}Ga_2$	4.4327(2)	–	–	5.0781(3)	–	–

The crystal structures of $SrGa_2$ and $BaGa_2$ were refined from single-crystal X-ray diffraction data, which are in good agreement with previously published results.[27] During the refinement strong anisotropic displacement of the Ga atoms was observed ($U_{33} > U_{11}$, Table 2). A similar observation was made in the high-pressure phase of $HoGa_2$.[28] An ordered deviation of the Ga atoms from the positions of the AlB_2-type structure was excluded using the structure model of the $CaIn_2$-type structure[13] and $EuGe_2$-type structure.[29] Inferior results were obtained for both of these models.

To model a static and statistic puckering of the Ga layers a split-atom model was used within the AlB_2-type structure. This results in a similar quality of the refinement to the AlB_2-type structure model considering anisotropic displacement of the atoms, but the anisotropy of displacement for the Ga atoms is significantly reduced. The displacement of the Ga atoms from the ideal position in the AlB_2-type structure is 0.086 and 0.071 Å for $SrGa_2$ and $BaGa_2$, respectively. In addition, we performed a refinement in space group *P*3*m*1, which did not improve the interpretation of the data.

Table 2. Atomic coordinates and displacement parameters (in Å^2) for $SrGa_2$ and $BaGa_2$ obtained by refinement of single-crystal X-ray diffraction data. The AlB_2-type and the AlB_2-type split-atom structure models were used for refinement (space group *P*6/*mmm*, lattice parameter cf. Table 1).

Atom	Site	*x*	*y*	*z*	U_{iso}	U_{11}	U_{33}
AlB_2-type model ($R_F = 0.055$)							
Sr	1*a*	0	0	0	0.0103(1)	0.0109(1)	0.0090(3)
Ga	2*d*	2/3	1/3	1/2	0.0106(1)	0.0073(1)	0.0174(3)
AlB_2-type split-atom model ($R_F = 0.055$)							
Sr	1*a*	0	0	0	0.0101(1)	0.0109(1)	0.0085(3)
Ga[a]	4*h*	1/3	2/3	0.5182(6)	0.0079(3)	0.0073(1)	0.0087(8)
AlB_2-type model ($R_F = 0.032$)							
Ba	1*a*	0	0	0	0.01204(6)	0.01232(8)	0.0115(1)
Ga	2*d*	2/3	1/3	1/2	0.01188(8)	0.00919(8)	0.0172(1)
AlB_2-type split-atom model ($R_F = 0.032$)							
Ba	1*a*	0	0	0	0.01234(6)	0.01230(8)	0.0114(1)
Ga[a]	4*h*	1/3	2/3	0.514(1)	0.0099(4)	0.00919(8)	0.011(1)

[a] Occupancy = 0.5.

Temperature-dependent single-crystal X-ray diffraction experiments have to be done to distinguish whether thermal motion of the atoms or static displacement is the origin of the anisotropic displacement parameter of the Ga atoms.

The intra- and interlayer distances of the Ga atoms resulting from the refinement of the single-crystal data using the AlB_2-type structure model are 2.51 and 4.74 Å for $SrGa_2$ and 2.56 and 5.08 Å for $BaGa_2$, respectively. In $CaGa_2$, crystallizing in the $CaIn_2$-type structure, the intra- and interlayer distances are 2.67 and 3.03 Å; and 4.36 Å, respectively.

$CaGa_2$ and $SrGa_2$ melt congruently at 989 and 1043 °C, respectively, in agreement with previous data.[5] $BaGa_2$ decomposes peritectically at 900 °C also in agreement with former investigations.[5] An endothermic effect at 597 °C for $CaGa_2$ can be assigned to a reversible phase transition to an AlB_2-type structure (space group *P*6*mmm*; lattice parameters: $a =$ 4.4296(7) Å, $c = 4.0740(9)$ Å, measured at $T = 650$ °C).

Chemical bonding in MGa_2 (M=Ca, Sr, and Ba): To characterize the chemical bonding of MGa_2 with M = Ca, Sr, and Ba, we analyzed the ELF based on FPLO calculations.

The topology of the ELF in $CaGa_2$ reveals two different interactions (Figure 2). The first one is visualized by the attractor with $\eta = 0.610$ located in the middle of the long Ga–Ga contact. The second one is represented by two attractors with $\eta = 0.569$ that are symmetrically located in the vicinity of the middle of the short Ga–Ga contact in the (002) plane. At slightly lower ELF values ($\eta = 0.548$) a ring-shaped domain forms around the center of the short Ga–Ga contact that reveals the reminiscent ring attractor, which may be expected in the case of the local cylindrical symmetry for an isolated Ga_2 molecule. The splitting of the ring attractor in $CaGa_2$ may be caused by the reduction of the local symmetry from the cylindrical due to the local atomic interactions. On the other hand a splitting of attractors with interconnecting ELF values close to that of the attractor may be a

 © 2009 Wiley-VCH Verlag GmbH & Co. KGaA, Weinheim

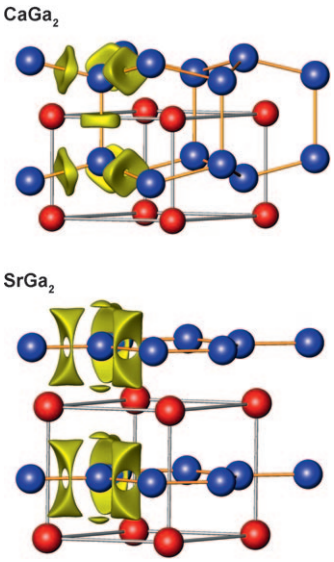

Figure 2. Isosurfaces of the ELF with $\eta = 0.525$ for the crystal structures of $CaGa_2$ and $SrGa_2$.

special feature of the FPLO method.[25] Integration of the total electron density within the basins of the two types of attractors yields 1.72 and 2.20 electrons per longer and shorter Ga–Ga contact, respectively. This implies bond orders of 0.86 and 1.1, respectively. The topology of the ELF and the bonding features in $CaGa_2$ are very similar to that in $YbGa_2$,[30] in which a bond order of 0.80 for the interlayer contact with d(Ga–Ga) = 3.009(2) Å and 1.05 for the intralayer contact with d(Ga–Ga) = 2.6696(7) Å were found.

By applying the integration of the electron density within the ELF basins, the charge transfer in calcium digallide may be illustrated by the following balance: $Ca^{2.32+}[Ga^{1.16-}]_2$, for example, roughly, $Ca^{2+}[Ga^{1-}]_2$.

The ELFs of $SrGa_2$ and $BaGa_2$ reveal very similar topologies different from that of $CaGa_2$ (Figure 2). Two ELF maxima are symmetrically located above and below each Ga–Ga contact within the planar 6^3 nets of Ga atoms. They form an elliptical domain at slightly lower ELF values than at the maximum. Additional attractors are found above and below each Ga atom, which are monosynaptic with respect to Ga atoms and may thus be understood as lone-pair-like. From the viewpoint of the ELF, individual 6^3 nets of Ga atoms are clearly separated from each other. The ELF interconnection value for basins of neighboring 6^3 nets is 0.187 and 0.118 for $SrGa_2$ and $BaGa_2$, respectively, which reflects a clear separation of the adjacent net basins.

Following the similar topology of the ELF in $SrGa_2$ and $BaGa_2$, an integration of the total electron density reveals 2.44 and 2.33 electrons per Ga–Ga bond and 0.56 and 0.64 electrons per lone pair in $SrGa_2$ and $BaGa_2$, respectively. The total charge balances can be written as $Sr^{2.44+}[Ga^{1.22-}]_2$ and $Ba^{2.28+}[Ga^{1.14-}]_2$, for example, $Sr^{2+}[Ga^{1-}]_2$ and $Ba^{2+}[Ga^{1-}]_2$, respectively.

The electron counts can be correlated with the interatomic distances in the crystal structures of the digallides of Ca, Sr, and Ba, as shown in Figure 3. For comparison, the values for $YbGa_2$ are also depicted. A general trend of shorter d-(Ga–Ga) distances with increasing electron count is clearly visible. Moreover, the relation between these two can be expressed by a formula similar to Pauling's bond-length–bond-order equation, $d(n) = d(1) - 0.71 \times \log(n)$ Å,[31] in which $d(n)$ is the bond length and n is half of the relevant electron count. The bond length for a Ga–Ga bond with an electron count of 2 resulting from least-squares fitting of the data is $d(1) = 2.77(2)$ Å, which is similar to that determined in an analysis of the ELF and interatomic distances in $YbGa_2$ ($CaIn_2$ type).[30] The observation of a correlation between interatomic distances and electron counts for Ga–Ga bonds contradicts the analysis for, for example, B–B bonds,[32] in which no such correlation was found. The reasons for this feature should be investigated later.

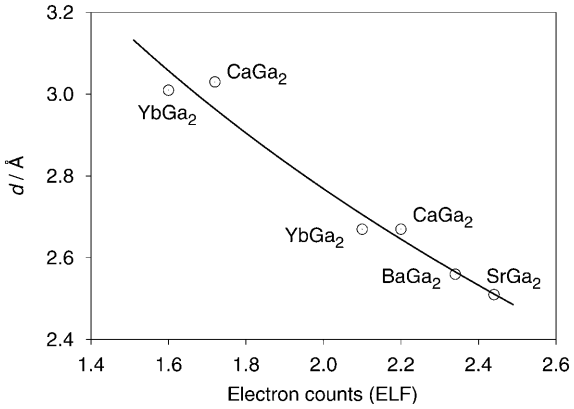

Figure 3. Correlation of electron counts determined by analysis of the ELF and interatomic distances (d) for MGa_2 with M = Yb, Ca, Sr, and Ba.

Alignment of the crystallites: During the NMR spectroscopy line-shape analysis distinct distortions of the expected regular powder pattern were observed. These are due to partial alignment of the crystallites in the magnetic field. The mechanism of the crystallite orientations in the magnetic field may have several origins. First, the crystallites have an anisotropic shape resulting in a preferred orientation during a possible sedimentation; this can be excluded by the irregular spherical shape of the crystallites after manually grinding the sample in a mortar, as observed by using an optical microscope and by the use of a viscous glue. The second reason could be a macroscopically induced current caused by a time-dependent magnetic field. This arises during the alignment process when the samples, suspended in glue, are introduced into the magnetic field. To exclude this mechanism samples were suspended in paraffin prior to the NMR spectroscopy experiments. The observed signal was identical to that measured on regular powders embedded in glue. After heating this sample in the magnetic field to 100 °C and

 © 2009 Wiley-VCH Verlag GmbH & Co. KGaA, Weinheim

cooling to 20 °C, a narrow NMR spectroscopy signal was observed, identical to that detected for samples embedded in glue and aligned in the magnetic field.

A similar orientation of the crystallites in a magnetic field was also observed in $Cu_{1-x}Al_2$ with $x=0.025$ in which the axis of alignment was parallel to the interpenetrating honeycomb-like 6^3 nets of the Al atoms.[33]

The origin of the reorientation of the crystallites in the magnetic field might result from a characteristic feature of the bonding situation being similar in both types of compounds. This is most probably the honeycomb-like covalently bonded nets of a distinct type of atom.

NMR spectroscopy: The ^{71}Ga and ^{69}Ga NMR spectroscopy signals of the title compounds are depicted in Figure 4. They are broadened by quadrupole coupling. The line shapes of the signals are in good agreement with those expected for the site symmetry of the Ga positions resulting in an axial symmetric EFG ($\eta_Q=0$). The quadrupole coupling constants determined by the frequency of the largest intensity singularities of the satellite transitions are summarized in Table 3. With consideration of the ratio of the nuclear quadrupole moments (Q) the results of the ^{71}Ga and ^{69}Ga experiments are in perfect agreement (Table 3). The quadrupole coupling constants are almost equal for $CaGa_2$ and $BaGa_2$ and become smaller with increasing radius of the cations for the isotypic compounds $SrGa_2$ and $BaGa_2$.

The main transitions show a characteristic frequency distribution described by second-order perturbation theory (Figure 5). A closer inspection of their line shape indicates the presence of a shift anisotropy, which can be most clearly seen in the shoulder at high frequencies for $BaGa_2$. The main transitions of the Ca and Sr compound are significantly smaller than predicted by the quadrupole coupling constant determined unambiguously from the satellite transitions. Least-squares fitting of the line shapes applying the quadrupole coupling constants obtained from the satellite transitions was used to determine the shift anisotropies. They increase with increasing size of the cations (Table 3).

The simulated ^{69}Ga main transition signals are in good agreement with the observed signals (Figure 5). The simulations are based on the parameter obtained in the ^{71}Ga experiments. This is an independent proof of the model obtained by analyzing the line shape of the ^{71}Ga NMR spectroscopy signals. Because of the larger quadrupole moment and the smaller magnetogyric ratio of ^{69}Ga relative to ^{71}Ga the ^{69}Ga NMR spectroscopy signals are dominated by quadrupole coupling, whereas in the ^{71}Ga NMR spectroscopy signals anisotropic shift interactions can be seen.

The signal shift is positive and does not relevantly change with M. Chemical shielding of Ga in diamagnetic insulators ranges from about −700 to 700 ppm.[34] This is significantly smaller than the signal shift in MGa_2 with M = Ca, Sr, and Ba, which indicates that the experimental shift is due to an interaction of the spins of the conduction electrons with the nuclear spins (Knight shift).

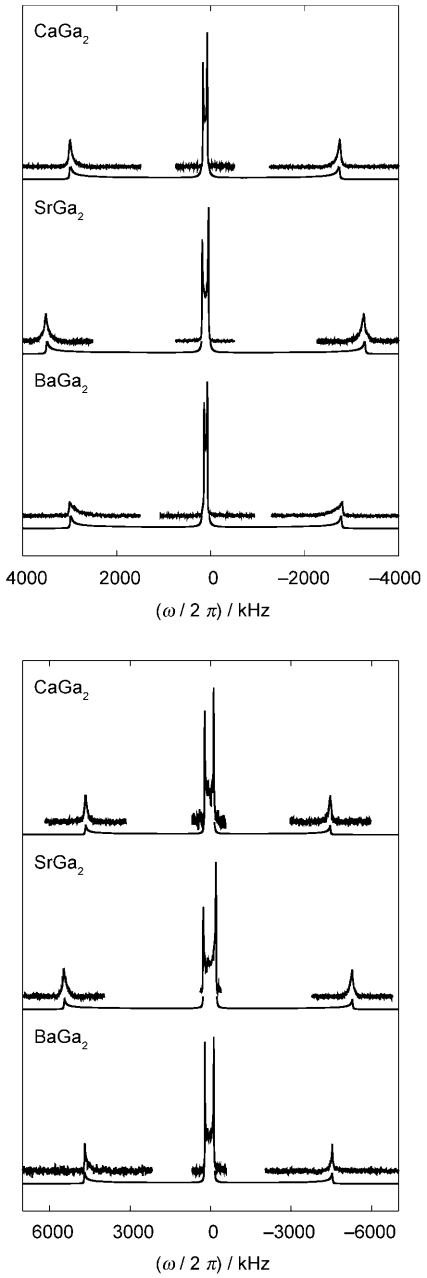

Figure 4. ^{71}Ga (top) and ^{69}Ga (bottom) NMR spectroscopy signals of regular powder of MGa_2 with M = Ca, Sr, and Ba. The signals are composed of experiments using three different carrier frequencies. The simulated signals are depicted below the experimental data.

A narrow signal at high frequencies was observed for magnetically oriented samples if the magnetic fields used for the alignment of the crystallites and the NMR spectroscopy experiment had the same direction (Figure 5). The narrow signals indicate a preferred orientation of the crystallites in the sample and the shift to the high frequency of the signals shows that the principal axis of the electric-field gradient (V_{ZZ}) is perpendicular to the magnetic field used for the measurements. Since the magnetic field applied for alignment of the crystallites is very homogeneous a random dis-

 © 2009 Wiley-VCH Verlag GmbH & Co. KGaA, Weinheim

Table 3. Signal shifts (Δ_{iso}), anisotropies of the shift (Δ_{aniso}), and coupling constants (C_Q) determined by ^{71}Ga and ^{69}Ga NMR spectroscopy lineshape analysis of the signals, and the ZZ component of the electric field gradient (V_{ZZ}). The experimental and average experimental values (exp), the calculated total (tot), and contributions of lattice (lat), total valence electrons (val), and p-like (pp), and d-like (dd) electrons[a] at the Ga site are given in 10^{21} V m^{-2}. Ratios of the occupation of the p_x-, p_y-, and p_z-like states, explained in the text, are also given.

	$CaGa_2$	$SrGa_2$	$BaGa_2$
	^{71}Ga NMR spectroscopy		
Δ_{iso} [ppm]	900(10)	910(10)	840(10)
Δ_{aniso} [ppm]	130(10)	150(10)	340(10)
C_Q [MHz]	11.5(1)	13.5(1)	11.6(1)
V_{ZZ}	4.44(4)	5.22(4)	4.48(4)
	^{69}Ga NMR spectroscopy		
C_Q [MHz]	18.3(1)	21.5(1)	18.4(1)
V_{ZZ}	4.43(3)	5.20(3)	4.45(3)
$<V_{ZZ}^{exp}>$	4.44(4)	5.21(4)	4.47(4)
V_{ZZ}^{tot}	3.77	4.13	4.38
V_{ZZ}^{lat}	−0.10	−0.14	−0.10
V_{ZZ}^{val}	3.87	4.27	4.48
V_{ZZ}^{val}(pp)	4.29	4.48	4.51
V_{ZZ}^{exp}(dd)	−0.47	−0.29	−0.09
$^1/_2[n(p_x)+n(p_y)]/n(p_z)$	1.182	1.208	1.224
$^1/_2[n(p_x)+n(p_y)]-n(p_z)$	0.051	0.050	0.053

[a] We use the notation given in ref. [17]. The valence contributions to the EFG originate from the nonspherical electron density within the atomic sphere and the lattice contribution to the EFG consists of charge density outside the considered atomic sphere.

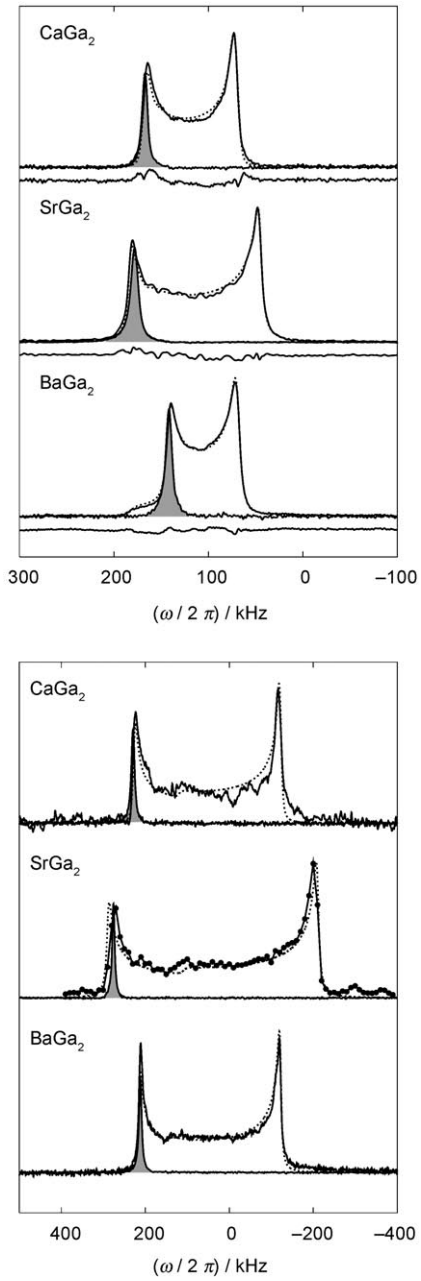

Figure 5. ^{71}Ga (top) and ^{69}Ga (bottom) NMR spectroscopy signals of the main transition of MGa_2 with M = Ca, Sr, and Ba. Solid lines represent the observed regular powder pattern. The simulated signals are symbolized by dashed lines. The difference between observed and calculated signals is shown below the signals for ^{71}Ga NMR spectroscopy experiments. The gray areas represent the signal of a powder oriented in a magnetic field.

tribution of V_{ZZ} in a plane perpendicular to the field can be expected. The ^{71}Ga NMR spectroscopy signals obtained for a variation of the orientation of this plane with respect to the magnetic field used for the measurement are depicted in Figure 6 for $BaGa_2$ as a function of α (angle of the minimum value between V_{ZZ} and the magnetic field used in the NMR spectroscopy experiment). Similar data were obtained for MGa_2 with M = Ca and Sr. For $\alpha \neq 90°$ a broadening of the signals was observed. The orientation dependence of the signals is proof that V_{ZZ} is randomly distributed in a plane perpendicular to the magnetic field used for the alignment of the crystallites. The simulation of the signals of the oriented powder was done by applying the coupling constants determined on the regular powder while considering the above-mentioned preferred orientation of the crystallites. The generation of the crystal files used for the SIMPSON simulations are explained in ref. [35].

Because of the point symmetry of the gallium position, V_{ZZ} is parallel to the [001] axis of the crystal structure and V_{XX} and V_{YY} are within in the Ga layers.

Magnetic susceptibility: Close to ambient temperature the magnetic susceptibility of the samples is independent of the applied field ($\mu_0 H > 1$ T), which demonstrates the absence of ferromagnetic impurities. At low temperatures the susceptibility in fields around 1 T shows small Curie-like contributions from minor paramagnetic impurities. Diamagnetic signals below 7.2 K and (stronger) below 6.0 K in low external fields are assumed to originate from the superconductivity of tiny gallium impurities not observed in the metallographic investigations. In general, $CaGa_2$ is diamagnetic, whereas both of the other digallides reveal paramagnetic behavior.

Whereas $CaGa_2$ and $SrGa_2$ feature an almost temperature-independent magnetic susceptibility behavior above 30 K ($\chi(T) = \chi_0$), the magnetic susceptibility of $BaGa_2$ increases slightly almost linearly with decreasing temperature

 © 2009 Wiley-VCH Verlag GmbH & Co. KGaA, Weinheim

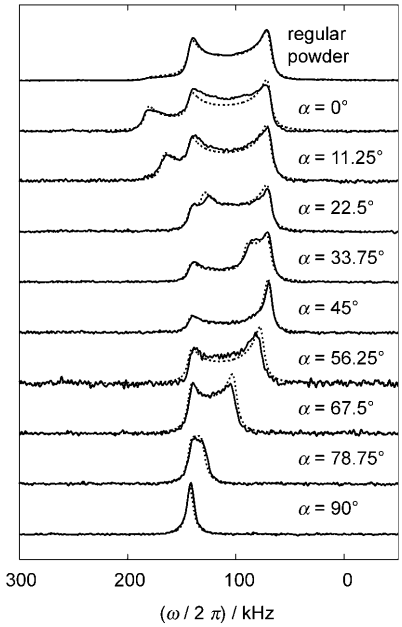

Figure 6. Orientation dependence of the ^{71}Ga NMR spectroscopy main transition signal of $BaGa_2$ powder aligned in a magnetic field. Solid lines represent the observed pattern. The simulated signals are symbolized by dashed lines. α is defined as the angle of the minimum value between V_{ZZ} and the magnetic field of the NMR spectroscopy experiment.

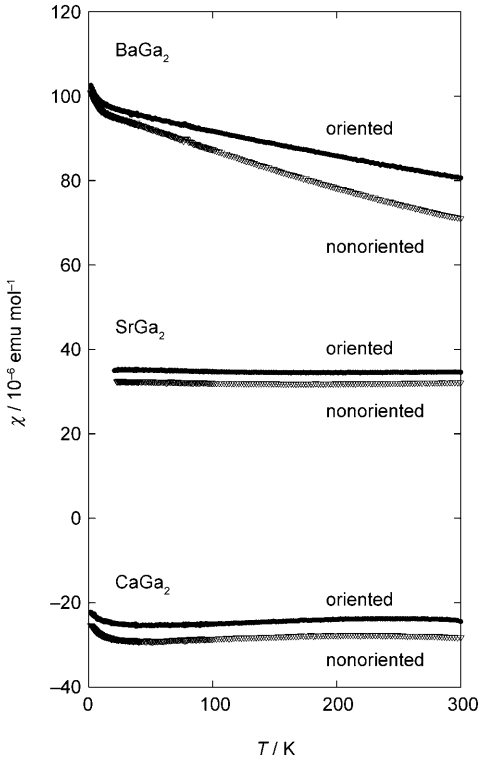

Figure 7. The magnetic susceptibility of MGa_2 with M = Ca, Sr, and Ba determined in a static field of $\mu_0 H = 3.5$ T.

(Figure 7). Extrapolation of $\chi(T)$ to $T = 0$ K (considering the Curie paramagnetic contribution) yields $\chi_0 = -29(20) \times 10^{-6}$, $+32(20) \times 10^{-6}$, and $+96(20) \times 10^{-6}$ emu mol^{-1} for the regular powders of Ca, Sr, and Ba compounds, respectively.

Taking into account the diamagnetic increment of the alkaline-earth ion, the resulting values for the polyanionic nets were corrected to $-21(20) \times 10^{-6}$, $+47(20) \times 10^{-6}$, and $+128(20) \times 10^{-6}$ emu mol^{-1}, respectively.

Samples oriented in the magnetic field generally have a larger magnetic susceptibility (by about 10×10^{-6} emu mol^{-1}) than those of regular powder of the digallides (Figure 7). Generally, this can be due to anisotropies of both the Pauli paramagnetic contribution and of the additional diamagnetic contribution.

Electronic structure: The lattice parameters obtained by the optimization procedure are summarized in Table 1. Optimized values are slightly smaller than those experimentally determined. The deviations are in the range typical for the LDA overbinding problem. The optimized z coordinate of the Ga atoms in $CaGa_2$ of 0.0447 is in perfect agreement with the experimentally observed coordinate of 0.0421(2) (ref. [27]).

The electronic density of states (DOS) of MGa_2 with M = Ca, Sr, and Ba is depicted in Figure 8. It can be split into three regions. The total DOS of $CaGa_2$ above -10 eV is dominated by the contributions of the Ga atoms. Region (I) ranges from -10 to -7.5 eV followed by a small pseudo gap separating this part from region (II) ranging from -7.5 to -4 eV. Region (III) below the Fermi level has, compared with the other regions, the largest contribution of the alkaline-earth metals. The Fermi level is located in a pseudo gap. A similar sequence is featured by $SrGa_2$ and $BaGa_2$ but regions (I) to (III) are slightly shifted to higher energies. The position of the Fermi level is on the high-energy shoulder for $SrGa_2$ followed by a wide range of low density of states. In $BaGa_2$ it is located on top of a flat maximum of the DOS, thus challenging the structural stability. This will be discussed later in detail.

The DOS values at the Fermi level (E_F) are 0.3, 1.5, and 2.5 states eV^{-1} f.u.$^{-1}$ (f.u. = formula units) for $CaGa_2$, $SrGa_2$, and $BaGa_2$, respectively. The values obtained within the free electron model from the Pauli paramagnetic susceptibility are 0.7, 1.6, and 4.3 states eV^{-1} f.u.$^{-1}$ for $CaGa_2$, $SrGa_2$, and $BaGa_2$, respectively (c.f. the magnetic susceptibility section). The values obtained by quantum mechanical calculations are in good agreement with those from the experiments. Experimental evaluation of the low-temperature electronic specific heat of $BaGa_2$ result in 3.0 states eV^{-1} f.u.$^{-1}$ also being in line.

Figure 8 (middle) shows the angular-momentum-decomposed electronic density of states of the Ga atoms of the investigated compounds. Regions (I) and (II) are dominated by the s-like states whereas region (III) is dominated by the p-like states. A significant overlap of the density of states of s- and p-like contributions exists in region (II). The contribution of the higher lying d-like states is very small and increases above the Fermi level for these compounds.

 © 2009 Wiley-VCH Verlag GmbH & Co. KGaA, Weinheim

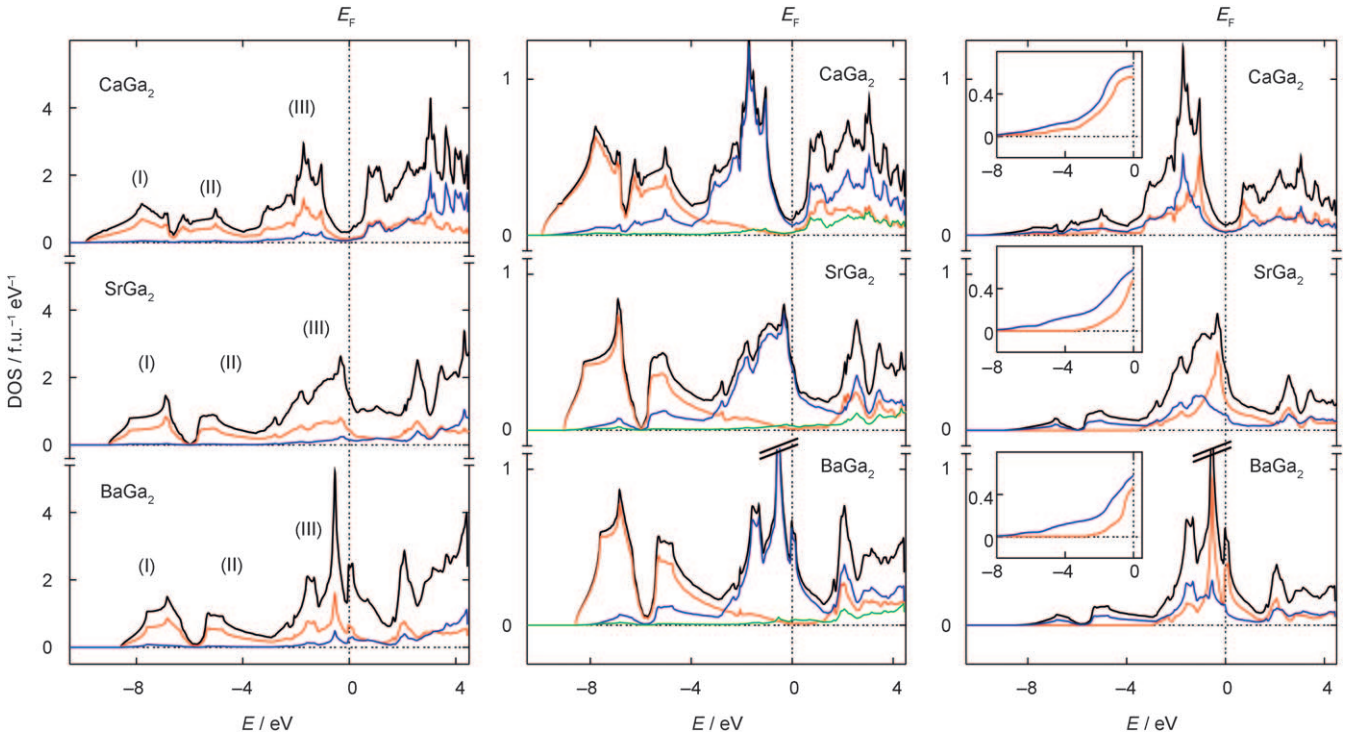

Figure 8. Electronic density of states (DOS) of MGa_2 with M = Ca, Sr, and Ba. Left: Total DOS and partial contributions of the atoms. Black lines represent the total DOS, red lines the Ga, and blue lines the M contributions. Regions (I) to (III) are discussed in the text. Middle: Angular-momentum-decomposed DOS of the Ga atoms. Black lines represent the total DOS of Ga, red lines the s, blue lines the p, and green lines the d contributions. Right: Angular-momentum-decomposed p-like DOS of Ga. Black lines represent the total p DOS of Ga, red lines the p_z, and blue lines the $^1/_2[(p_x)+(p_y)]$ contributions. The integrated DOS of both contributions is shown in the insets by red lines for $n(p_z)$ and blue lines for $^1/_2[n(p_x)+n(p_y)]$.

The occupation of electronic states at the Fermi level indicates metallic behavior of the compounds. This justifies the interpretation that the shift of the NMR spectroscopy signals is due to Knight shift (c.f. the NMR spectroscopy section). The occupations of the s-like states of the Ga atoms at the Fermi level are 0.007, 0.004, and 0.004 states atom^{-1} eV^{-1} for $CaGa_2$, $SrGa_2$, and $BaGa_2$, respectively. The small and similar numbers of the s-like states at the Fermi level is in agreement with the—relative to other metals—small and almost equal experimental Knight shift of the NMR spectroscopy signals (Table 3).

The distributions of the Fermi velocities of the electrons are anisotropic and similar for $SrGa_2$ and $BaGa_2$ (AlB_2-type), and differ only slightly for $CaGa_2$ with a $CaIn_2$-type structure (Figure 9). The Fermi velocities of the electrons can be decomposed into fast in-plane (001) and slow out-of-plane contributions. A minimization of the Lorentz force ($\vec{F} = q\vec{v} \times \vec{B}$) is achieved for an orientation of the crystallites with the (001) plane parallel to the direction of the magnetic field applied for the alignment of the crystallites. This corresponds to the preferred orientation of the crystallites observed in the NMR spectroscopy experiments.

From the analysis of the orbital characters we find that the (001) in-plane contributions to the high Fermi velocities are due to the p_x- and p_y-like states. Furthermore, a hybridization of the s-, p_x-, and p_y-like states is indicated. The electron transport in MGa_2 with M = Ca, Sr, and Ba proceeds by means of the Ga–Ga p_x- and p_y-like electrons, whereas the

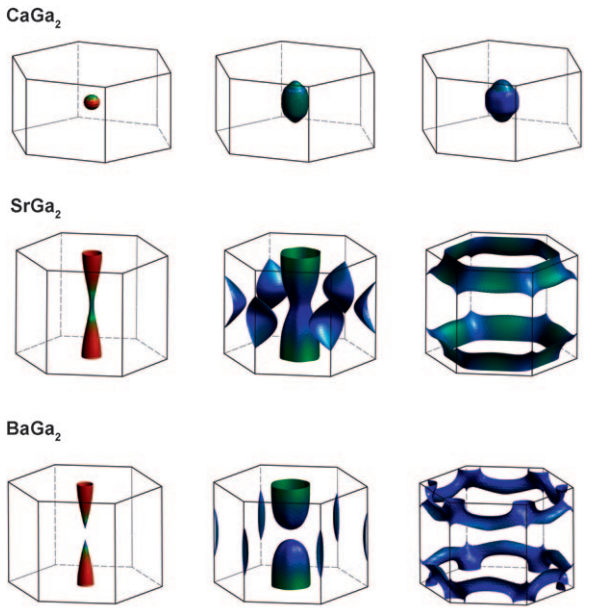

Figure 9. Fermi surfaces for different bands of MGa_2 with M = Ca, Sr, and Ba. Red and blue indicate high and low Fermi velocities, respectively.

 © 2009 Wiley-VCH Verlag GmbH & Co. KGaA, Weinheim

p_z-like electrons have less influence. The situation is different to MgB_2 in which the electric conductivity is due to the p_z-like electrons, whereas the p_x- and p_y-like electrons cause the superconductivity.[36]

The calculated values of V_{ZZ} and the different contributions are summarized in Table 3. V_{ZZ} is dominated by the local contributions of the electrons, for example, the local basis of the Ga atoms, whereas the contributions of the lattice, built by all atoms regardless of the atom being considered, and the interstitial region are small. The p-like electrons have a much larger effect on V_{ZZ} than the d-like electrons. The s-like electrons do not have a contribution due to the spherical symmetry of the s-wave functions.

The positive sign of V_{ZZ} is due to a larger occupation of p_x- and p_y-like states compared with the p_z-like states. This can be seen by analysis of the angular-momentum-decomposed integrated DOS of the Ga atoms for energies below E_F (Figure 8, right). A similar observation was made for transition elements with *hcp* crystal structures, in which the change of the sign of V_{ZZ} was accompanied by a change in the difference of the occupation of p_x- and p_y-like to p_z-like states ($\Delta n(p) = {}^1/_2[n(p_x)+n(p_z)]$).[17] The ratio $({}^1/_2[n(p_x)+n(p_y)])/n(p_z)$ follows the tendency of the calculated V_{ZZ} for MGa_2 with M = Ca, Sr, and Ba, whereas $\Delta n(p)$ indicates only the sign of V_{ZZ} (Table 3).

The total values of V_{ZZ} are in good agreement with the results of the NMR spectroscopy measurements for $CaGa_2$ and $BaGa_2$. The deviation of $-21\,\%$ for $SrGa_2$ is larger than expected (usually in the range of $\pm 15\,\%$). This may indicate a deviation of the crystal structure from AlB_2-type, which is also indicated by the anisotropy of the displacement parameters of the Ga atoms.

Total energy calculations using the $CaIn_2$-type structure model and the corresponding lattice parameter of $SrGa_2$ in the AlB_2-type structure show, for a variation of the z parameter of the Ga atoms, that the minimum is obtained for a displacement of 0.125 Å (Figure 10). Neither the position of the minimum of energy nor the energy difference significantly changes within the LDA or GGA approximation for an optimized and experimental lattice parameter. The shift of the Ga atoms is in line with the value of 0.086 Å determined by X-ray diffraction using a split-atom model (cf. crystal chemistry section). The energy difference of a displacement of the Ga atoms between 0 and 0.125 Å is about 0.01 eV, which is significantly below the thermal energy at ambient temperature. Therefore, the $CaIn_2$-type structure is not observed at ambient temperature because no static order in that position can be expected for such a flat potential-energy curve. Motional narrowing[15,19] averaging the quadrupole coupling has not to be considered because the orientation of the PAS with respect to the applied magnetic field does not change due to symmetry restrictions.

An increase of V_{ZZ} of $SrGa_2$ with an increase of the z parameter is observed for the $CaIn_2$-type structure model (Figure 10, inset). For a Ga displacement of 0.125 Å the value of $V_{ZZ} = 4.86 \times 10^{21}\,V\,m^{-2}$ is in a good agreement with

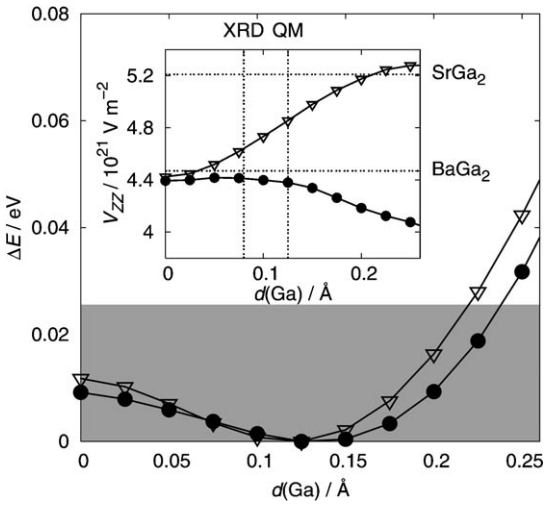

Figure 10. Energy deviation for displacement of the Ga atoms in the $CaIn_2$-type structure. ● represent the values calculated for $BaGa_2$ and ▽ for $SrGa_2$. The thermal energy at ambient temperature is indicated by the gray area. Inset: Variation of V_{ZZ} with displacement of the Ga atoms. The results of the NMR spectroscopy experiments are marked by horizontal lines. The vertical lines represent the Ga displacement determined by single-crystal XRD and QM calculations.

V_{ZZ} determined in the NMR spectroscopy experiments (Table 3).

Applying the $CaIn_2$-type structure model to $BaGa_2$ results in a similar behavior (Figure 10). A minimum of the energy is calculated for a Ga displacement of 0.125 Å compared with 0.071 Å determined by X-ray diffraction. However, the EFG does not significantly change within the range of $0 \leq d(Ga) \leq 0.125$ Å (Figure 10, inset). The results of the NMR spectroscopy experiments are well reproduced by the quantum mechanical calculations when considering the displacement of the Ga atoms. An analysis of the density of states using the $CaIn_2$-type model for $BaGa_2$ shows a shift of the maximum that is located at E_F to lower energies for the AlB_2-type structure.

From considering the results of single-crystal X-ray diffraction and NMR spectroscopy experiments as well as the results of the quantum mechanical calculations, the structure models of $SrGa_2$ and $BaGa_2$ have to be modified. The close match of V_{ZZ} determined from NMR spectroscopy experiments and quantum mechanical calculations obtained only using the $CaGa_2$-type structure model indicates a puckering of the Ga layers. Due to the small energy difference of the shifted and the nonshifted Ga atoms, a nonordered puckering of the Ga layers can be expected, as actually observed from the single-crystal X-ray diffraction experiments. Measurements of the heat capacity of $BaGa_2$ do not display any structural change in the range between 1.8 and 320 K.

Conclusion

Analysis of the crystallographic information reveals that in the series of digallides of the alkaline-earth metals MGa_2

 © 2009 Wiley-VCH Verlag GmbH & Co. KGaA, Weinheim

(M = Ca, Sr, and Ba) the crystal structure changes from the $CaIn_2$-type for M = Ca to the AlB_2-type for M = Sr and Ba. The primitive hexagonal arrangement of the M atoms remains unchanged, and its axis ratio increases strongly proceeding from $CaGa_2$ to $SrGa_2$ and only slightly for $SrGa_2$ to $BaGa_2$. Gallium atoms form three shorter and one longer contact in $CaGa_2$, and only three shorter contacts in the other digallides. Topological analysis of the electron localization function in $CaGa_2$ shows clearly that, despite the relatively large interatomic distance of 3.03 Å, the longer Ga–Ga contact is also a bonding one. From the point of view of chemical bonding, the structural transformation from $CaGa_2$ to $SrGa_2$ ($BaGa_2$) is reflected in the polyanionic part formed by the four-bonded gallium atoms in $CaGa_2$ and the three-bonded gallium atoms in the two other digallides. The reorganization of the polyanion changes the electronic density of states around the Fermi level: in $CaGa_2$ it locates in a pseudo gap with low DOS, in $SrGa_2$ and $BaGa_2$ the pseudo gap disappears and the DOS values at E_F are much higher. This tendency is clearly confirmed by measurements of the magnetic susceptibility: $CaGa_2$ is diamagnetic, whereas Sr and Ba reveal paramagnetic behavior. Additional support for the bonding models was obtained by ^{69,71}Ga NMR spectroscopy, which revealed a nonmonotonic change of the width of the main transition signal increasing from $CaGa_2$ to $SrGa_2$ and decreasing to $BaGa_2$. Experimentally obtained and calculated DOS values at the Fermi level are in good agreement, which shows the consistency of the calculated electronic structure.

The Knight shift of the NMR spectroscopy signals does not change with the cations and the crystal structure in good agreement with the small and not strongly varying s-like contributions of the Ga atoms to the DOS at the Fermi level in MGa_2 compounds. The anisotropy of the signal shift is not significantly influenced by the change of the crystal structure and follows the increase of the size of the cations and the unit-cell volume. The quadrupole coupling constants increase first from $CaGa_2$ to $SrGa_2$, following the changes in the Ga polyanion, and decrease further to $BaGa_2$. The absolute values of the electric-field gradient determined precisely from the NMR spectroscopy data are in fair agreement with the calculated values for $CaGa_2$ and $BaGa_2$ and differ strongly for $SrGa_2$.

A deviation of the crystal structure of $SrGa_2$ from the AlB_2-type motive in the form of a puckering of the Ga nets is shown by the improved agreement of the observed and calculated EFG using the $CaIn_2$-type structure model. For $BaGa_2$ the same modification of the structure model results in a shift of a peak at the Fermi level observed for the AlB_2-type structure model towards lower energies. The calculated displacement of the Ga atoms in $SrGa_2$ and $BaGa_2$ of about ± 0.125 Å along the [001] axis is in line with crystallographic data.

The calculated Fermi velocities are strongly anisotropic for both structural motives, being largest in the (001) plane and remarkably reduced along the [001] axis. This results in an anisotropy of the electronic transport taking place predominantly parallel to the honeycomb-like planes formed by the strongly covalently bonded Ga atoms. Experimentally this is expressed in the alignment of the crystallites in the magnetic field with the [001] axis perpendicular to the field vector, as revealed by the ^{69,71}Ga NMR spectroscopy and magnetic susceptibility data.

Acknowledgements

We gratefully acknowledge the assistance of Susann Leipe during synthesis of the samples. Furthermore, we thank Dr. Ulrich Burkhard for metallographic investigations and Dr. Stefan Hoffmann and Susann Müller for thermal analysis of the samples. In addition, we thank Dr. Peter Jeglič for fruitful discussion. This work was partially supported by the DFG SPP 1178 (Katrin Koch) and the Emmy Noether-Programm (Dr. Helge Rosner).

[1] H. Schäfer, B. Eisenmann, W. Müller, *Angew. Chem.* **1973**, *85*, 742; *Angew. Chem. Int. Ed.* **1973**, *12*, 694.
[2] M. L. Fornasini, M. Pani, *Acta Crystallogr. Sect. C* **1986**, *42*, 394.
[3] M. L. Fornasini, F. Merlo, *Rev. Chim. Miner.* **1979**, *16*, 458.
[4] M. L. Fornasini, *Acta Crystallogr. Sect. C* **1983**, *39*, 943.
[5] G. Bruzzone, *Boll. Sci. Fac. Chim. Ind. Bologna* **1966**, *24*, 113.
[6] F. Haarmann, Y. Prots, *Z. Anorg. Allg. Chem.* **2006**, *632*, 2135.
[7] S. Cirafici, M. L. Fornasini, *J. Less-Common Met.* **1990**, *163*, 331.
[8] O. Sichevych, R. Ramlau, R. Giedigkeit, M. Schmidt, R. Niewa, Yu. Grin, *Abstracts 13th Int. Conf. Solid Compounds of Transition Elements* **2000**, Stresa, O-13.
[9] O. Sichevych, Y. Prots, Yu. Grin, *Z. Kristallogr. New Cryst. Struct.* **2006**, *221*, 265.
[10] F. Haarmann, Y. Prots, S. Göbel, H. G. von Schnering, *Z. Kristallogr. New Cryst. Struct.* **2006**, *221*, 257.
[11] G. Bruzzone, M. L. Fornasini, F. Merlo, *J. Less-Common Met.* **1989**, *154*, 67.
[12] W. Hofmann, W. Jäniche, *Naturwissenschaften* **1935**, *23*, 851.
[13] A. Iandelli, *Z. Anorg. Allg. Chem.* **1964**, *330*, 221.
[14] B. D. Sharma, J. Donohue, *Z. Kristallogr.* **1962**, *117*, 293.
[15] C. P. Slichter, *Principles of Magnetic Resonance*, 3rd ed., Springer, Berlin, **1990**.
[16] P. Herzig, *Theor. Chim. Acta* **1985**, *67*, 323.
[17] O. Blaha, K. Schwarz, P. H. Dederichs, *Phys. Rev. B* **1988**, *37*, 2792.
[18] M. Bak, J. T. Rasmussen, N. C. Nielsen, *J. Magn. Reson.* **2000**, *147*, 296.
[19] A. Abragam, *Principles of Nuclear Magnetism*, Oxford University, Oxford, **1961**.
[20] R. K. Harris, E. D. Becker, *J. Magn. Reson.* **2002**, *156*, 323.
[21] K. Koepernik, H. Eschrig, *Phys. Rev. B* **1999**, *59*, 1743.
[22] J. P. Perdew, Y. Wang, *Phys. Rev. B* **1992**, *45*, 13244.
[23] P. Blaha, K. Schwarz, G. Madsen, D. Kvasnicka, J. Luitz, K. Schwarz, WIEN2k: An Augmented Plane Wave Local Orbitals Program for Calculating Crystal Properties, Technische Universität Wien, **2001**.
[24] A. Savin, H. J. Flad, J. Flad, H. Preuss, H. G. von Schnering, *Angew. Chem.* **1992**, *104*, 185; *Angew. Chem. Int. Ed. Engl.* **1992**, *31*, 185.
[25] A. Ormeci, H. Rosner, F. R. Wagner, M. Kohout, Yu. Grin, *J. Phys. Chem. A* **2006**, *110*, 1100.
[26] M. Kohout, Basin: Version 2.4, Max-Planck-Institut für Chemische Physik fester Stoffe, Dresden, **2006**.
[27] W. Harms, M. Wendorff, C. Röhr, *Z. Naturforsch. B* **2007**, *62b*, 177.
[28] U. Schwarz, S. Bräuninger, Yu. Grin, K. Syassen, M. Hanfland, *J. Alloys Compd.* **1998**, *268*, 161.
[29] E. I. Gladyshevskii, *J. Struct. Chem.* **1964**, *5*, 523.
[30] U. Schwarz, R. Giedigkeit, R. Niewa, M. Schmidt, W. Schnelle, R. Cardoso, M. Hanfland, Z. Hu, K. Klementiev, Yu. Grin, *Z. Anorg. Allg. Chem.* **2001**, *627*, 2249.

 © 2009 Wiley-VCH Verlag GmbH & Co. KGaA, Weinheim

[31] L. Pauling, *The Chemical Bond*, Cornell University, Ithaca, **1967**.
[32] A. M. Alekseeva, A. M. Abakumov, P. S. Chizhov, A. Leithe-Jasper, W. Schnelle, Y. Prots, J. Hadermann, E. V. Antipov, Yu. Grin, *Inorg. Chem.* **2007**, *46*, 7378.
[33] F. Haarmann, M. Armbrüster, Yu. Grin, *Chem. Mater.* **2007**, *19*, 1147.
[34] J. Mason, *Multinuclear NMR*, Kluwer Academic, Milton Keynes, **1987**.
[35] Unpublished results (F. Haarmann and P. Jeglič): Only the polar angle (θ) has to be considered to generate the crystal files used for SIMPSON simulations of oriented samples in the present case since $\eta_Q = \eta_\Delta = 0$. It can be shown that θ has to be substituted by $\arccos(\cos(\alpha) \times \cos(\varphi))$ with φ being uniformly distributed between 0 and 180°. About 2001 crystallite orientations were used to obtain the presented simulations.
[36] P. C. Canfield, G. W. Crabtree, *Phys. Today* **2003**, *56*, 34.

Received: June 10, 2008
Revised: September 26, 2008
Published online: January 2, 2009

 © 2009 Wiley-VCH Verlag GmbH & Co. KGaA, Weinheim